

High Dynamic Range Image Quality Assessment Based on Frequency Disparity

Yue Liu, *Student Member, IEEE*, Zhangkai Ni, *Member, IEEE*, Shiqi Wang, *Senior Member, IEEE*,
Hanli Wang, *Senior Member, IEEE*, and Sam Kwong, *Fellow, IEEE*

Abstract—In this paper, a novel and effective image quality assessment (IQA) algorithm based on frequency disparity for high dynamic range (HDR) images is proposed, termed as local-global frequency feature-based model (LGFMM). Motivated by the assumption that the human visual system is highly adapted for extracting structural information and partial frequencies when perceiving the visual scene, the Gabor and the Butterworth filters are applied to the luminance of the HDR image to extract local and global frequency features, respectively. The similarity measurement and feature pooling are sequentially performed on the frequency features to obtain the predicted quality score. The experiments evaluated on four widely used benchmarks demonstrate that the proposed LGFMM can provide a higher consistency with the subjective perception compared with the state-of-the-art HDR IQA methods. Our code is available at: <https://github.com/eezkni/LGFMM>.

Index Terms—Image quality assessment (IQA), High dynamic range (HDR), Gabor feature, Butterworth feature.

I. INTRODUCTION

WITH the rapid development of imaging technology and the growing demand for immersive experiences, the high dynamic range (HDR) images are increasingly indispensable due to the realistic experiences they can provide, which can significantly contribute to the development of TV and photography industry. Compared with the 8-bit low dynamic range (LDR) images, HDR images are linearly related to the physical luminance in the scene and can record more structural details by using 16-32 bit floating point values [1]. Essentially speaking, there are two major differences between HDR and LDR images, 1) the data distribution of HDR images is much broader than that of LDR images; 2) more detailed structures can be preserved in HDR images. Therefore, most image quality assessment (IQA) methods designed for LDR images are not suitable for direct use in assessing the quality of HDR images, which makes it crucial for developing effective IQA models for HDR images.

The IQA models aim to objectively evaluate the image quality to align with the human visual system (HVS). As a fundamental problem in the field of image processing, IQA models have been widely used to optimize the performance of various learning-based vision tasks and to improve image

encoding capability by increasing compression ratio while preserving the original image quality. According to the amount of available information of the reference image, existing IQA models can be roughly divided into three categories, full-reference (FR) [2] [3], reduced-reference (RR) [4] [5], and no-reference (NR) [6] [7]. In this paper, we are committed to proposing a novel and effective FR IQA model for HDR images.

The most widely used objective IQA measure for HDR images is the HDR visual difference predictor (HDR-VDP) proposed by Mantiuk *et al.* [8], the latest release of which is HDR-VDP-3 [9]. They model the HVS by taking into account optical and retinal pathways in the human eye and evaluating visible differences between images. The dynamic range independent metric (DRIM) proposed by Aydin *et al.* [10] models the HVS and presents the differences with three distortion maps, which is difficult for subsequent analysis due to the lack of a pooling strategy. Currently, there is a metric specifically designed for the HDR video content, namely HDR video quality metric (HDR-VQM) proposed by Narwaria *et al.* [11]. The input HDR video sequences are first projected to the perceptual domain, then the Gabor filter is applied to extract the frequency features, which are used to calculate the subband errors. The final quality score is obtained through spatial and temporal pooling. Nevertheless, both the HDR-VDP-3 and the HDR-VQM require additional viewing information such as display parameters and viewing distance.

Due to the lack of IQA measures specifically designed for HDR images, various objective LDR IQA models are also used to evaluate the quality of HDR images. However, the data distribution of the HDR image is quite different from that of the LDR image. Since traditional CRFs are designed for dim LDR displays, Aydin *et al.* [12] proposes the perceptual uniform (PU) space to map a wide range of luminance to a perceptual range that is consistent with the HVS. Therefore, the quality of encoded HDR images can be evaluated with LDR measures, such as peak signal-to-noise ratio (PSNR), structural similarity (SSIM) [13], gradient magnitude similarity deviation (GMSD) [14], visual information fidelity (VIF) [15], and feature similarity (FSIM) [16]. In analogous to the PU function, the perceptual quantizer (PQ) proposed in [17] can be used in the same way. HDR-Combination of Quality Metrics (HDR-CQM) proposed by Choudhury [18] improves the performance of HDR IQA by taking advantage of various HDR and LDR IQA metrics. Recently, Mikhailiuk *et al.* [19] construct a Unified Photometric Image Quality dataset (UPIQ) by aligning and merging two HDR and two

Yue Liu, Shiqi Wang and Sam Kwong are with the Department of Computer Science, City University of Hong Kong. (e-mail: yliu724-c@my.cityu.edu.hk; shiqiwang@cityu.edu.hk; cssamk@cityu.edu.hk).

Zhangkai Ni and Hanli Wang are with the Department of Computer Science and Technology, Key Laboratory of Embedded System and Service Computing (Ministry of Education), and Shanghai Institute of Intelligent Science and Technology, Tongji University, Shanghai 200092, P. R. China (e-mail: eezkni@gmail.com; hanliwang@tongji.edu.cn).

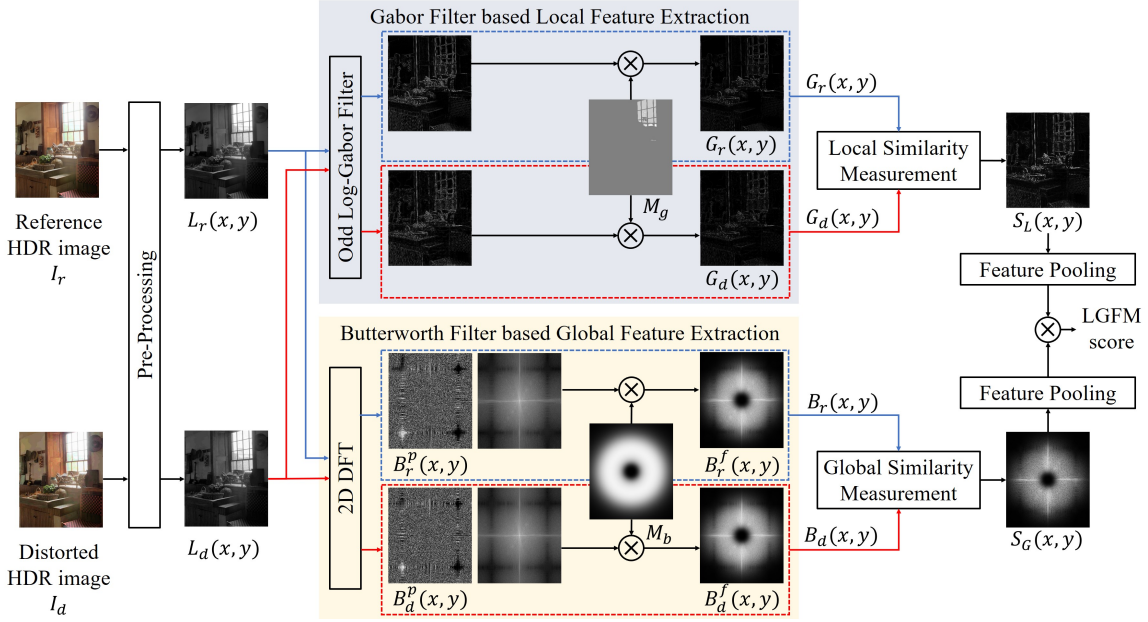


Fig. 1. The flowchart of the proposed *Local and Global Frequency feature-based Model (LGFM)* for HDR IQA. Firstly, The reference and distorted HDR images, I_r and I_d , are converted to the luminance perceptual space, L_r and L_d , in the pre-processing stage. Subsequently, an odd log-Gabor filter is designed to extract local frequency features, G_r and G_d , with a spatial mask M_g used to provide higher weights to the over-exposed region. Meanwhile, the Butterworth filter is used to simulate the contrast sensitivity function to highlight the sensitive frequency interval in HVS by the generated mask M_b . The global frequency features of the reference and distorted HDR images, B_r and B_d , are consisted of the corresponding phase maps and the weighted frequency maps. Finally, the local and global similarities are measured, followed by the feature pooling strategy to predict the quality score.

LDR image datasets for IQA, based on which the PU-PieAPP model is trained for HDR IQA.

In this paper, a novel full-reference HDR IQA metric is constructed by modeling the HVS-sensitive information with local and global frequency characters to further improve the assessment accuracy. The proposed *Local and Global Frequency feature-based Model (LGFM)* is mainly inspired by two observations. First, the local frequency feature can well represent the texture details perceived by human eyes. Second, the global frequency feature can be used to characterize the sensitive frequency interval of the HVS. In the proposed method, the reference and distorted HDR images are first transferred to the perceptual space using the PU coding. Thereafter, local and global frequency feature maps are extracted by specifically designed Gabor filtering and Butterworth filtering, respectively. The similarity measurements and pooling strategies are performed on the feature maps to generate similarity scores of local and global frequency features, respectively. The final prediction quality score is obtained by multiplying these two scores. Abundant experiments demonstrate the superiority of the proposed LGFM in the evaluation of the HDR image quality compared with the state-of-the-art IQA algorithms.

II. PROPOSED LOCAL AND GLOBAL FREQUENCY FEATURE-BASED MODEL

The framework of the proposed LGFM is illustrated in Fig. 1, which consists of four processing stages. Firstly, the reference and distorted HDR image, I_r and I_d , are converted to the perceptual space in the pre-processing stage. The corresponding luminance maps, $L_r(x,y)$ and $L_d(x,y)$, are obtained from the linear luminance space by the PU coding, where (x,y) denotes the pixel coordinate in the image. In the

second stage, the Gabor filter and Butterworth filter are used to extract the local frequency features ($G_r(x,y)$, $G_d(x,y)$) and global frequency features ($B_r(x,y)$, $B_d(x,y)$), respectively. In the third stage, the computed frequency features from the reference and distorted HDR images are compared separately to yield the local and global similarity maps. Finally, the two computed similarity maps are combined to generate the predicted quality score using the proposed feature pooling strategies.

A. Gabor Filter-based Local Feature Extraction

The local frequency feature can be used to extract abundant structural and edge information, where the Gabor filter is greatly consistent with the response of the HVS [13], [20], [21]. Therefore, we adopt the Gabor filter for local frequency feature extraction. The Gabor filter-based features of reference and distorted HDR images are denoted as $G_r(x,y)$ and $G_d(x,y)$, respectively.

Inspired by work [21], the local edge information is extracted using the odd log-Gabor filter, which can well represent the high-frequency component of nature images,

$$G_o(x,y) = \frac{1}{2\pi\sigma_x\sigma_y} \exp \left\{ \frac{-1}{2} \left[\log \left(\frac{x'}{\sigma_x} \right)^2 + \log \left(\frac{y'}{\sigma_y} \right)^2 \right] \right\} \sin(2\pi f x'), \quad (1)$$

where

$$\begin{aligned} x' &= x\cos\theta + y\sin\theta; \\ y' &= y\cos\theta - x\sin\theta, \end{aligned} \quad (2)$$

where f and θ denote the frequency and the rotation angle of (x',y') . The standard deviations of the Gaussian envelope in

the two directions are represented as σ_x and σ_y , respectively. More specifically, in this work, the rotation angle is set to 0 and $\pi/2$ to extract horizontal and vertical edge features, respectively, and the frequency f is empirically set to 2.5. Furthermore, the HDR images can provide abundant texture information in the bright areas, which enables it to provide the better visual experience compared with the LDR image. Therefore, a spatial mask is applied on the extracted local features, focusing on the high luminance region of HDR images. The designed Gaussian function is applied to obtain the mask,

$$M_g = 1 + \frac{1}{2\pi\sigma} \exp\left(\frac{-(L_r) - \mu)^2}{2\sigma^2}\right), \quad (3)$$

where σ and μ are empirically set to 0.2 and 250. It is worth mentioning that all feature extraction operations in this work are performed on the luminance of HDR images unless otherwise stated.

B. Butterworth Filter-based Global Feature Extraction

Over the past few decades, frequency features have been widely adopted to extract the local texture or edge information of the nature images [21], [22]. However, the direct difference in the frequency domain between the reference and distorted images has not been extensively discussed. Furthermore, the contrast sensitivity of the human eye first increases and then decreases with the increase of spatial frequency [23], which implies that there is a frequency interval where HVS is highly sensitive. Motivated by this observation, this paper adopts the Butterworth filter to simulate the *contrast sensitivity function* (CSF) to directly extract the global feature from the frequency spectrum of the image. Given a 2D image, each pixel of its frequency representation is computed from all the pixels in its spatial domain. Therefore, the frequency representation of an image can be regarded as a global feature of the image. Taking the reference HDR image as an example, the corresponding 2D *Discrete Fourier transform* (DFT) is performed as:

$$F_r(u, v) = \sum_{x=0}^{M-1} \sum_{y=0}^{N-1} L_r(x, y) e^{-j2\pi(ux/M + vy/N)}, \quad (4)$$

where M and N are the size of the image, (u, v) denotes the pixel coordinate in the frequency spectrum. After shifting the low frequencies to the middle of the frequency spectrum, the log operation is applied to compress the values for better representation. Subsequently, a bandpass Butterworth filter is designed to provide higher weights to the special frequency interval,

$$M_b = \left(1 - \frac{1}{1 + (D_1/D)^{2n_1}}\right) \cdot \left(\frac{1}{1 + (D_2/D)^{2n_2}}\right), \quad (5)$$

where D is the Euclidean distance of the 2D grid. In this work, the cut-off frequency and order value D_1 , D_2 , n_1 , and n_2 are empirically set to 400, 100, 4 and 2, respectively. The masked frequency map is presented as,

$$B_r^f(x, y) = \log(|F_r(u, v)| + 1) \cdot M_b. \quad (6)$$

Moreover, by separating the frequency spectrum into real and imaginary part, i.e., $R_r = \text{Real}(F_r)$ and $I_r = \text{Imag}(F_r)$,

the phase map can be obtained as $B_r^p = \tan^{-1}(I_r/R_r)$. In the same way, the frequency map B_d^f and phase map B_d^p of the distorted HDR image can be obtained. Therefore, the Butterworth filter-based global feature is composed of the frequency map and phase map, which is given by,

$$\begin{aligned} B_r(x, y) &= \{B_r^f(x, y), B_r^p(x, y)\}; \\ B_d(x, y) &= \{B_d^f(x, y), B_d^p(x, y)\}. \end{aligned} \quad (7)$$

C. Feature Similarity Measurements

Since the generated local and global frequency features are represented in different domains, the feature similarity measurements are conducted on the spatial and frequency domains, respectively. The similarity map of the local frequency features is calculated as follows:

$$S_L(x, y) = \frac{2G_r(x, y) \cdot G_d(x, y) + T_0}{G_r(x, y)^2 + G_d(x, y)^2 + T_0}, \quad (8)$$

where the T_0 is a positive constant to prevent the exception that the denominator equals to zero.

For the global feature, the similarity of the frequency map and phase map can be generated as,

$$\begin{aligned} S_g^f(x, y) &= \frac{2B_r^f(x, y) \cdot B_d^f(x, y) + T_1}{B_r^f(x, y)^2 + B_d^f(x, y)^2 + T_1}; \\ S_g^p(x, y) &= \frac{2B_r^p(x, y) \cdot B_d^p(x, y) + T_2}{B_r^p(x, y)^2 + B_d^p(x, y)^2 + T_2}, \end{aligned} \quad (9)$$

where the T_1 and T_2 are the positive constants, in analogous to T_0 . The final similarity map of the global frequency feature is obtained as,

$$S_G(x, y) = [S_g^f(x, y)]^\alpha \cdot [S_g^p(x, y)]^{(1-\alpha)}, \quad (10)$$

where α is a positive constant used for weighting control of $S_g^f(x, y)$ and $S_g^p(x, y)$. In this work, T_0 , T_1 , T_2 , and α are empirically set as 0.014, 8, 1, and 0.5, respectively.

D. Feature Pooling

In feature maps generated from HDR images using the Gabor filter and Butterworth filter, the larger pixel value implies that the HVS is more sensitive and pays more attention to it. Therefore, the weighted maps for the local and global frequency feature maps can be generated as:

$$\begin{aligned} W_G(x, y) &= \max\{|G_r(x, y)|, |G_d(x, y)|\}; \\ W_L(x, y) &= \max\{|B_r^f(x, y)|, |B_d^f(x, y)|\}. \end{aligned} \quad (11)$$

Therefore, the local frequency similarity score and global frequency similarity score can be calculated as the weighted average over all the pixel locations (x, y) on the corresponding similarity maps as:

$$\begin{aligned} Q_G(x, y) &= \sum_{(x, y)} W_G(x, y) \cdot S_G(x, y) / \sum_{(x, y)} W_G(x, y); \\ Q_L(x, y) &= \sum_{(x, y)} W_L(x, y) \cdot S_L(x, y) / \sum_{(x, y)} W_L(x, y). \end{aligned} \quad (12)$$

The final quality score is obtained by combining the local similarity score and global frequency similarity score,

$$Q_{LGFM} = Q_G(x, y) \cdot Q_L(x, y). \quad (13)$$

TABLE I
SROCC, KROCC AND RMSE COMPARISON OF VARIOUS IQA MODELS ON FOUR WIDELY USED BENCHMARKS.

Criteria		SROCC					KROCC					RMSE				
Dataset		D-V	D-Z	D-N	UPIQ	Avg.	D-V	D-Z	D-N	UPIQ	Avg.	D-V	D-Z	D-N	UPIQ	Avg.
HDR-VQM		0.8965	0.7611	0.7248	0.8888	0.8178	0.7031	0.5621	0.5649	0.7002	0.6326	12.2101	18.8356	0.8189	0.3819	8.0616
HDR-VDP-3		0.9132	0.7558	0.8467	0.8214	0.8343	0.7392	0.5698	0.6718	0.6421	0.6557	10.7257	19.6734	0.5470	0.4089	7.8388
SSIM	PU	0.8699	0.7827	0.7057	0.7369	0.7738	0.6719	0.5787	0.5332	0.5488	0.5832	14.0147	18.7897	0.8298	0.5258	8.5400
	PQ	0.8736	0.7682	0.6508	0.7315	0.7560	0.6850	0.5783	0.4870	0.5486	0.5747	14.5140	19.4345	0.8665	0.5132	8.8321
MSSIM	PU	0.9009	0.8004	0.8377	0.8063	0.8363	0.7261	0.6098	0.6622	0.6113	0.6524	12.1315	29.1735	0.7774	0.5162	10.6497
	PQ	0.8994	0.8417	0.8299	0.8118	0.8457	0.7113	0.6458	0.6529	0.6197	0.6574	11.8489	15.8932	0.7801	0.5023	7.2561
PSNR	PU	0.6672	0.6591	0.6131	0.6311	0.6426	0.4797	0.4760	0.4517	0.4582	0.4664	22.6432	21.8065	0.8581	0.5208	11.4572
	PQ	0.6681	0.6476	0.6198	0.6327	0.6421	0.4797	0.4623	0.4571	0.4588	0.4645	21.3461	20.0826	0.8619	0.5147	10.7013
GMSD	PU	0.8918	0.8738	0.8080	0.7784	0.8380	0.7064	0.6919	0.6224	0.5824	0.6508	12.0439	13.4912	0.6487	0.4357	6.6549
	PQ	0.8846	0.8719	0.7979	0.7696	0.8310	0.6900	0.6886	0.6134	0.5735	0.6414	12.3418	13.6594	0.6798	0.4550	6.7840
FSIM	PU	0.9090	0.8337	0.8323	0.7693	0.8361	0.7376	0.6571	0.6525	0.5702	0.6544	11.8094	15.4822	0.7790	0.5258	7.1491
	PQ	0.9064	0.8358	0.8213	0.7648	0.8321	0.7392	0.6583	0.6401	0.5669	0.6511	11.7802	15.5461	0.8005	0.5378	7.1662
VIF	PU	0.9183	0.8284	0.6705	0.7640	0.7953	0.7372	0.6737	0.5067	0.5838	0.6254	11.4667	17.3586	0.7338	0.4233	7.4956
	PQ	0.9158	0.8283	0.6631	0.7568	0.7910	0.7307	0.6753	0.4977	0.5761	0.6200	11.4650	18.2018	0.7442	0.4309	7.7105
ESIM	PU	0.9176	0.8866	0.7763	0.8559	0.8591	0.7392	0.7137	0.5932	0.6762	0.6806	12.4762	13.8699	0.6487	0.3565	6.8378
	PQ	0.9139	0.8836	0.7685	0.8529	0.8547	0.7392	0.7088	0.5863	0.6720	0.6766	12.5785	13.7950	0.6480	0.3518	6.8433
GFM	PU	0.9052	0.9154	0.7182	0.7848	0.8309	0.7162	0.7485	0.5400	0.5890	0.6484	11.7361	10.8275	0.7617	0.4494	5.9437
	PQ	0.8984	0.9088	0.7119	0.7693	0.8221	0.7113	0.7359	0.5380	0.5738	0.6398	11.9960	17.8278	0.7922	0.4767	7.7732
LGFm	PU	0.9200	0.9322	0.8539	0.9032	0.9023	0.7491	0.7707	0.6824	0.7236	0.7315	10.6462	10.5293	0.5392	0.3097	5.5061
	PQ	0.9195	0.9207	0.8611	0.8928	0.8985	0.7458	0.7634	0.6833	0.7070	0.7249	11.4299	10.9682	0.5523	0.3072	5.8144

III. EXPERIMENTAL RESULTS

A. HDR Dataset and Evaluation Protocols

In this section, four publicly available datasets are used for performance evaluation [24] [25] [26] [27]. The first three datasets are constructed by subjective experiments, while the fourth dataset consists of two existing datasets using a specifically designed algorithm to align subjective scores [26] [28].

As suggested in the VQEG HDTV test [29] [30], a logistic regression function is applied to map the predicted objective scores to a common scale,

$$S_i = \gamma_1 \left(\frac{1}{2} - \frac{1}{1 + e^{\gamma_2(q_i - \gamma_3)}} \right) + \gamma_4 q_i + \gamma_5, \quad (14)$$

where q_i and S_i denote the generated quality score of the i -th image from the IQA model and the corresponding mapped score. γ_1 , γ_2 , γ_3 , γ_4 , and γ_5 are the regression parameters determined by minimizing the sum of squared differences between the predicted objective score S_i and corresponding ground truth score (i.e., MOS/DMOS). Subsequently, the Spearman rank order correlations coefficient (SROCC), Kendall rank order correlation coefficient, and root mean square error (RMSE) are adopted to evaluate the performance of various HDR IQA metrics. Note that higher values of SROCC and KROCC represent a stronger correlation, while lower values of RMES indicate smaller differences.

B. Performance Comparison

To illustrate the superiority of the proposed LGFM, several classic and state-of-the-art IQA metrics are adopted for comparison, including HDR-VDP-3 [9], HDR-VQM [11], PSNR, SSIM [13], FSIM [16], VIF [15], GMSD [14], ESIM [20], GFM [21], and MSSIM [31], where the first two algorithms are specifically designed for HDR images, while the other metrics are for LDR images. Therefore, HDR images are first converted into perceptual space by PU or PQ coding before

TABLE II

ABLATION STUDY TO EXPLORE THE ROLE OF THE LOCAL AND GLOBAL FREQUENCY FEATURES, AS WELL AS THE MASKS M_g AND M_b .

		Dataset	L	L w/o M_g	G	G w/o M_b	LGFm
SROCC	D-V	0.9139	0.9137	0.9163	0.9131	0.9200	
	D-Z	0.9249	0.9244	0.9234	0.9128	0.9322	
	D-N	0.8355	0.8382	0.8484	0.8346	0.8539	
	UPIQ	0.8717	0.8707	0.8982	0.8516	0.9032	
KROCC	D-V	0.7409	0.7392	0.7376	0.7310	0.7491	
	D-Z	0.7574	0.7561	0.7537	0.7319	0.7707	
	D-N	0.6575	0.6593	0.6768	0.6577	0.6824	
	UPIQ	0.6831	0.6816	0.7230	0.6617	0.7236	
RMSE	D-V	11.0598	11.1183	11.5351	14.3446	10.6462	
	D-Z	10.7154	10.7952	11.3910	13.7609	10.5293	
	D-N	0.5556	0.5535	0.5431	0.6718	0.5392	
	UPIQ	0.3210	0.3227	0.3114	0.3945	0.3097	

applying the LDR IQA metrics. Since the parameters in part of the IQA models (i.e., display and distance parameters in HDR-VDP-3 and HDR-VQM) would affect the final results, we use the default settings during the experiments.

Table I presents the performance comparison of various IQA models on four datasets, where the highlighted in bold with red, blue, and black represent the first, second, and third-ranked performance of the measurement criterions. Compared with the state-of-the-art IQA metrics, our proposed LGFM model yields the best overall performance in terms of SROCC, KROCC, and MSE on four datasets. Besides, the HDR-VDP-3, HDR-VQM, and PU-GFM also achieved relatively promising results. Moreover, there is an interesting observation that most of the highlighted values are from PU coding, which indicates that PU encoding performs higher consistency with the HVS compared with the PQ coding.

C. Ablation Study

This subsection verifies the effectiveness of each component in the proposed LGFM model, including the Gabor filter-based local feature, Butterworth filter-based global feature, as well as

the proposed two masks M_g and M_b . More specifically, four LGFM variants are conducted as follows: 1) L: only Gabor filter-based local frequency feature is used for evaluation. 2) L w/o M_g : removing the weighting mask M_g in L. 3) G: only Butterworth filter-based global frequency feature is used for evaluation. 4) G w/o M_b : removing the weighting mask M_b in G. It is worth mentioning that PU coding is adopted in our model. As shown in Table II, both the M_g and M_b contribute to feature extraction in L and G, respectively, which illustrate the effectiveness of the over-exposed regions and the frequency interval. Furthermore, the combination of local and global frequency features outperforms using either one alone, indicating that the proposed two feature maps achieve complementarity between local and global frequency features.

IV. CONCLUSIONS

This paper proposes the LGFM model, a novel image quality assessment algorithm for HDR images. The key contribution of our model lies in the combination of the local and global frequency features. More specifically, the local feature map is extracted by the Gabor filter to measure the structure similarity, while the global feature map is obtained by simulating the *contrast sensitivity function* with the Butterworth filter to detect the frequency interval similarity. Subsequently, the feature pooling strategy is adopted to generate the quality scores based on the local and global similarity maps, leading to the final quality score by combing them. Extensive experiments demonstrate that each component in the proposed LGFM contributes to the final results. Moreover, the proposed model provides higher consistency with the HVS and outperforms other state-of-the-art IQA models.

REFERENCES

- [1] F. Dufaux, P. Le Callet, R. Mantiuk, and M. Mrak, *High dynamic range video: from acquisition, to display and applications*. Academic Press, 2016.
- [2] Y. Fu, H. Zeng, L. Ma, Z. Ni, J. Zhu, and K.-K. Ma, "Screen content image quality assessment using multi-scale difference of gaussian," *IEEE Transactions on Circuits and Systems for Video Technology*, vol. 28, no. 9, pp. 2428–2432, 2018.
- [3] Y. Tian, H. Zeng, J. Hou, J. Chen, J. Zhu, and K.-K. Ma, "A light field image quality assessment model based on symmetry and depth features," *IEEE Transactions on Circuits and Systems for Video Technology*, vol. 31, no. 5, pp. 2046–2050, 2020.
- [4] S. Wang, K. Gu, X. Zhang, W. Lin, S. Ma, and W. Gao, "Reduced-reference quality assessment of screen content images," *IEEE Transactions on Circuits and Systems for Video Technology*, vol. 28, no. 1, pp. 1–14, 2016.
- [5] Z. Huang and S. Liu, "Perceptual hashing with visual content understanding for reduced-reference screen content image quality assessment," *IEEE Transactions on Circuits and Systems for Video Technology*, vol. 31, no. 7, pp. 2808–2823, 2020.
- [6] F.-Z. Ou, Y.-G. Wang, J. Li, G. Zhu, and S. Kwong, "A novel rank learning based no-reference image quality assessment method," *IEEE Transactions on Multimedia*, 2021.
- [7] Z. Pan, F. Yuan, J. Lei, Y. Fang, X. Shao, and S. Kwong, "Vcrnet: Visual compensation restoration network for no-reference image quality assessment," *IEEE Transactions on Image Processing*, vol. 31, pp. 1613–1627, 2022.
- [8] R. Mantiuk, K. J. Kim, A. G. Rempel, and W. Heidrich, "Hdr-vdp-2: A calibrated visual metric for visibility and quality predictions in all luminance conditions," *ACM Transactions on graphics (TOG)*, vol. 30, no. 4, pp. 1–14, 2011.
- [9] M. Narwaria, R. Mantiuk, M. P. Da Silva, and P. Le Callet, "Hdr-vdp-2.2: a calibrated method for objective quality prediction of high-dynamic range and standard images," *Journal of Electronic Imaging*, vol. 24, no. 1, p. 010501, 2015.
- [10] T. O. Aydın, R. Mantiuk, K. Myszkowski, and H.-P. Seidel, "Dynamic range independent image quality assessment," *ACM Transactions on Graphics (TOG)*, vol. 27, no. 3, pp. 1–10, 2008.
- [11] M. Narwaria, M. P. Da Silva, and P. Le Callet, "Hdr-vqm: An objective quality measure for high dynamic range video," *Signal Processing: Image Communication*, vol. 35, pp. 46–60, 2015.
- [12] T. O. Aydın, R. Mantiuk, and H.-P. Seidel, "Extending quality metrics to full luminance range images," in *Human vision and electronic imaging xiii*, vol. 6806. SPIE, 2008, pp. 109–118.
- [13] Z. Wang, A. C. Bovik, H. R. Sheikh, and E. P. Simoncelli, "Image quality assessment: from error visibility to structural similarity," *IEEE transactions on image processing*, vol. 13, no. 4, pp. 600–612, 2004.
- [14] W. Xue, L. Zhang, X. Mou, and A. C. Bovik, "Gradient magnitude similarity deviation: A highly efficient perceptual image quality index," *IEEE transactions on image processing*, vol. 23, no. 2, pp. 684–695, 2013.
- [15] H. R. Sheikh, A. C. Bovik, and G. De Veciana, "An information fidelity criterion for image quality assessment using natural scene statistics," *IEEE Transactions on image processing*, vol. 14, no. 12, pp. 2117–2128, 2005.
- [16] L. Zhang, L. Zhang, X. Mou, and D. Zhang, "Fsim: A feature similarity index for image quality assessment," *IEEE transactions on Image Processing*, vol. 20, no. 8, pp. 2378–2386, 2011.
- [17] S. Standard, "High dynamic range electro-optical transfer function of mastering reference displays," *SMPTE ST*, vol. 2084, no. 2014, p. 11, 2014.
- [18] A. Choudhury, "Robust hdr image quality assessment using combination of quality metrics," *Multimedia Tools and Applications*, vol. 79, no. 31, pp. 22 843–22 867, 2020.
- [19] A. Mikhailiuk, M. Pérez-Ortiz, D. Yue, W. Suen, and R. K. Mantiuk, "Consolidated dataset and metrics for high-dynamic-range image quality," *IEEE Transactions on Multimedia*, vol. 24, pp. 2125–2138, 2021.
- [20] Z. Ni, L. Ma, H. Zeng, J. Chen, C. Cai, and K.-K. Ma, "ESIM: Edge similarity for screen content image quality assessment," *IEEE Transactions on Image Processing*, vol. 26, no. 10, pp. 4818–4831, 2017.
- [21] Z. Ni, H. Zeng, L. Ma, J. Hou, J. Chen, and K.-K. Ma, "A gabor feature-based quality assessment model for the screen content images," *IEEE Transactions on Image Processing*, vol. 27, no. 9, pp. 4516–4528, 2018.
- [22] C.-L. Yang, W.-R. Gao, and L.-M. Po, "Discrete wavelet transform-based structural similarity for image quality assessment," in *2008 15th IEEE International Conference on Image Processing*. IEEE, 2008, pp. 377–380.
- [23] P. G. Barten, "Formula for the contrast sensitivity of the human eye," in *Image Quality and System Performance*, vol. 5294. SPIE, 2003, pp. 231–238.
- [24] G. Valenzise, F. De Simone, P. Lauga, and F. Dufaux, "Performance evaluation of objective quality metrics for hdr image compression," in *Applications of Digital Image Processing XXXVII*, vol. 9217. SPIE, 2014, pp. 78–87.
- [25] E. Zerman, G. Valenzise, and F. Dufaux, "An extensive performance evaluation of full-reference hdr image quality metrics," *Quality and User Experience*, vol. 2, no. 1, pp. 1–16, 2017.
- [26] M. Narwaria, M. P. Da Silva, P. Le Callet, and R. PÉpion, "Impact of tone mapping in high dynamic range image compression," in *VPQM*, 2014, pp. pp–1.
- [27] A. Mikhailiuk, M. Perez-Ortiz, W. Suen, and R. Mantiuk, "Upiq: Unified photometric image quality dataset," 2020.
- [28] P. Korshunov, P. Hanhart, T. Richter, A. Artusi, R. Mantiuk, and T. Ebrahimi, "Subjective quality assessment database of hdr images compressed with jpeg xt," in *2015 seventh international workshop on quality of multimedia experience (QoMEX)*. IEEE, 2015, pp. 1–6.
- [29] V. Q. E. Group *et al.*, "Final report from the video quality experts group on the validation of objective models of video quality assessment," in *VQEG meeting, Ottawa, Canada, March, 2000*, 2000.
- [30] H. R. Sheikh, M. F. Sabir, and A. C. Bovik, "A statistical evaluation of recent full reference image quality assessment algorithms," *IEEE Transactions on image processing*, vol. 15, no. 11, pp. 3440–3451, 2006.
- [31] Z. Wang, E. P. Simoncelli, and A. C. Bovik, "Multiscale structural similarity for image quality assessment," in *The Thirty-Seventh Asilomar Conference on Signals, Systems & Computers*, 2003, vol. 2. Ieee, 2003, pp. 1398–1402.